Formation Mechanism of Porous Single-Crystal Cr_2O_3 and Co_3O_4 Templated by Mesoporous Silica

Calum Dickinson,[†] Wuzong Zhou,*[,†] Robert P. Hodgkins,[‡] Yifeng Shi,[§] Dongyuan Zhao,[§] and Heyong He[§]

School of Chemistry, University of St. Andrews, St. Andrews, Fife KY16 9ST, United Kingdom, Department of Physical, Inorganic and Structural Chemistry, Arrhenius Laboratory, Stockholm University, SE-106 91 Stockholm, Sweden, and Department of Chemistry and Shanghai Key Laboratory of Molecular Catalysis and Innovative Materials, Fudan University, Shanghai 200433, P. R. China.

Received January 3, 2006. Revised Manuscript Received March 21, 2006

Porous single crystals of Cr_2O_3 and Co_3O_4 templated by mesoporous silicas, SBA-15 and KIT-6, have been fabricated. Specimens at different stages of crystal growth were characterized by using XRD and high-resolution transmission electron microscopy. The final products of oxide porous single crystals were also characterized by nitrogen adsorption/desorption experiments. A multiseed formation mechanism can eventually be established. The present investigation revealed that the original mesostructures in SBA-15 and KIT-6 were negatively replicated by the crystals of oxides, and therefore, the dimension of the building blocks (nanorods or nanowires) in the porous crystals of oxides depends on the pore diameter of the silica. It was also found that a mesopore system, regarded as a nanoreactor, had a significant influence on the size and morphology of produced oxide particles and on the route and temperature of the crystallization.

1. Introduction

Ordered mesoporous materials were first discovered in the early 1990s by Mobil scientists.[1,2] The simple soft templating method by using organic surfactants, which form micelles in aqueous solutions, allows for a wide range of mesoporous materials to be synthesized. Over the past 14 years, many reports have been published on new phases of mesoporous silica including SBA-15, KIT-6, and FDU series,[3−7] functionalized mesoporous silicas,[8] mesoporous metals,[9] mesoporous thin films,[10] and mesoporous metal oxides.[11] Mesoporous metal oxides are of wide interest for applications in catalysis since they can be regarded as self-supported catalysts with large specific surface areas and shape selective properties. These materials can be synthesized by using either organic soft templates, similar to the synthesis of mesoporous silica, or mesoporous silica as a hard template. While soft templating normally results in amorphous materials, due to the low decomposition temperature of the template, hard templating allows for crystalline materials to be formed. The hard templating method was first introduced by Ryoo and co-workers,[12] and several mesoporous carbon, metals, metal sulfides, and metal oxides have been fabricated, although the wall of most of these materials was still disordered and the formation mechanisms of these new materials were not discussed extensively.

In our previous report, we demonstrated that porous single crystals (PSCs) of Cr_2O_3 and WO_3 can be prepared using mesoporous silica SBA-15 as the hard template and using $H_2Cr_2O_7$ and $H_3PW_{12}O_{40}$ as the precursors, respectively.[13,14] Recently, synthesis of Co_3O_4, In_2O_3, and Cr_2O_3 PSCs with a cubic double pyramidal channel system was also achieved.[15−17] In the present work, we synthesized porous single crystals of Cr_2O_3 and Co_3O_4 using SBA-15 and KIT-6 as templates

* To whom correspondence should be addressed. E-mail: wzhou@st-andrews.ac.uk. Tel: +44 1334 467276. Fax: +44 1334 463808.
† University of St. Andrews.
‡ Stockholm University.
§ Fudan University.

(1) Kresge, C. T.; Leonowicz, M. E.; Roth, W. J.; Vartuli, J. C.; Beck, J. S. *Nature* **1992**, *359*, 710.
(2) Beck, J. S.; Vartuli, J. C.; Roth, W. J.; Leonowicz, M. E.; Kresge, C. T.; Schmitt, K. D.; Chu, C. T.-W.; Olsen, D. H.; Sheppard, E. W.; McCullen, S. B.; Higgins, J. B.; Schlenker, J. L. *J. Am. Chem. Soc.* **1992**, *114*, 10834.
(3) Zhao, D. Y.; Huo, Q. S.; Feng, J. L.; Chmelka, B. F.; Stucky, G. D. *J. Am. Chem. Soc.* **1998**, *120*, 6024.
(4) Kleitz, F.; Choi, S. H.; Ryoo, R. *J. Chem. Soc., Chem. Commun.* **2003**, 2136.
(5) Liu, X. Y.; Tian, B. Z.; Yu, C. Z.; Gao, F.; Xie, S. H.; Tu, B.; Che, R. C.; Peng, L. M.; Zhao, D. Y. *Angew. Chem., Int. Ed.* **2002**, *41*, 3876.
(6) Fan, J.; Yu, C. Z.; Gao, F.; Lei, J.; Tian, B.; Wang, L.; Luo, Q.; Tu, B.; Zhou, W. Z.; Zhao, D. Y. *Angew. Chem., Int. End.* **2003**, *42*, 3146.
(7) Fan, J.; Yu, C. Z.; Lei, J.; Zhung, Q.; Li, T. C.; Tu, B.; Zhou, W. Z.; Zhao, D. Y. *J. Am. Chem. Soc.* **2005**, *127*, 10794.
(8) Jaroniec, C. P.; Kruk, M.; Jaroniec, M.; Sayari, A. *J. Phys. Chem. B* **1998**, *102*, 5503.
(9) Terasaki, O.; Liu, Z.; Ohsuna, T.; Shin, H. J.; Ryoo, R. *Microsc. Microanal.* **2002**, *8*, 35.
(10) Brinker, C. J.; Lu, Y. F.; Sellinger, A.; Fan, H. Y. *Adv. Mater.* **1999**, *11*, 579.
(11) Yang, P. D.; Zhao, D. Y.; Margolese, D. I.; Chmelka, B. F.; Stucky, G. D. *Nature* **1998**, *396*, 152.
(12) Ryoo, R.; Joo, S. H.; Jun, S. *J. Phys. Chem. B* **1999**, *103*, 7743.
(13) Zhu, K. K.; Yue, B.; Zhou, W. Z.; He, H. Y. *Chem. Commun.* **2003**, 98.
(14) Yue, B.; Tang, H. L.; Kong, Z. P.; Zhu, K. K.; Dickinson, C.; Zhou, W. Z.; He, H. Y. *Chem. Phys. Lett.* **2005**, *407*, 83.
(15) Jiao, K.; Zhang, B.; Yue, B.; Ren, Y.; Liu, S. X.; Yan, S. R.; Dickinson, C.; Zhou, W. Z.; He, H. Y. *Chem. Commun.* **2005**, 5618.
(16) Tian, B. Z.; Liu, X. Y.; Solovyov, L. A.; Liu, Z.; Yang, H. F.; Zhang, Z. D.; Xie, S. H.; Zhang, F. Q.; Tu, B.; Yu, C. Z.; Terasaki, O.; Zhao, D. Y. *J. Am. Chem. Soc.* **2004**, *126*, 865.
(17) Tian, B. Z.; Liu, X. Y.; Yang, H. F.; Xie, S. H.; Yu, C. Z.; Tu, B.; Zhao, D. Y. *Adv. Mater.* **2003**, *15*, 1370.

10.1021/cm060014p CCC: $33.50
Published on Web 06/03/2006

and chromium/cobalt nitrates as precursors. SBA-15 contains close hexagonally packed straight mesopores connected by some smaller channels and micropores,[3] while KIT-6 has a cubic mesostructure, space group $Ia\bar{3}d$, which contains three-dimensional (3D) bicontinuous channel networks.[4] The formation mechanisms of these crystal growths were studied by the examination of the intermediate products of the early-stage crystal growth.[18,19] A significant confinement effect on the crystal growth in the mesopore systems was discovered.

2. Experimental Section

Synthesis of PSC Co_3O_4 in KIT-6 was performed by using a modified method according to that reported previously by Tian et al.[16] A 0.50 g portion of cobalt nitrate hexahydrate was dissolved in 6.5 g ethanol and stirred with 0.15 g of KIT-6, which was freshly prepared according to literature,[4] for 2 h. The ethanol was then evaporated off at approximately 40 °C. During the process of ethanol evaporation, the metal nitrates were drawn into the pores by capillary action. The cobalt nitrate was then thermally decomposed at 550 °C for 5 h, with a temperature heating rate of 2 °C/min from room temperature, and cobalt oxide crystals grew inside the KIT-6 channels. The KIT-6 silica framework was then removed by dissolving it in an aqueous 10 wt % HF solution. The remaining powder was washed with water thrice after centrifuging and decanting off the clear solution. To study the phase transformation at an early stage of crystal growth, a series of specimens were collected after the $Co(NO_3)_2{\cdot}6H_2O$-loaded mesoporous silica was heated for 5 h at 125−200 °C with intervals of 25 °C, and at 150 °C for 0.5−2 h in 0.5 h steps. To compare the crystal growth behaviors of cobalt oxide, thermal decomposition of $Co(NO_3)_2{\cdot}6H_2O$ in air without using a silica template was also performed at various temperatures.

For growing PSC Cr_2O_3, chromium(III) nitrate nonahydrate was substituted for cobalt nitrate. Both SBA-15 and KIT-6 were used as templates. The reaction temperature for $Cr(NO_3)_3{\cdot}9H_2O$-loaded SBA-15 was increased from room temperature to 500 °C with 50 °C steps, so that a series of intermediate specimens could be collected for further investigation. Another series of specimens were collected for more detailed investigation after the precursor sample was heated at 350 °C with different time from 0.5 to 2 h with intervals of 0.5 h. Again, nontemplate chromium nitrate nonahydrate was decomposed at different temperatures, and the intermediate phases were collected.

Characterization of specimens was initially carried out using X-ray powder diffraction (XRD) on a Philips reflective diffractometer with Cu Kα radiation ($\lambda = 0.15418$ nm). The microstructures of the specimens were examined by high-resolution transmission electron microscopy (HRTEM) on a JEOL JEM-2011 electron microscope operated at 200 kV. The powder specimen for TEM examination was ground, suspended in acetone, and deposited on a copper specimen grid supported by a holey carbon film. TEM images were recorded with a Gatan 794 CCD camera at magnifications of 60000× to 1000000×. The compositions of the specimens were analyzed using energy-dispersive X-ray spectroscopy (EDX).

A Micromeritics ASAP 2020 instrument was used for nitrogen adsorption measurements. Samples were degassed at 120 °C for 2 h once the final temperature had been reached prior to analysis typically measured at 77 K consisting of an adsorption and desorption branch. Specific surface areas were calculated via the BET model in regions applicable to the derivation of the model between P/P_0 values of 0.05−0.4. The total pore volume was estimated from the uptake of nitrogen at a relative pressure of $P/P_0 = 0.99$. Pore size distribution curves were obtained from the NLDFT model assuming cylindrical pore geometry for the silica hard-template and slit geometry for the PSCs and *t*-plots with thickness curves using the Broekhoff−De Boer model.

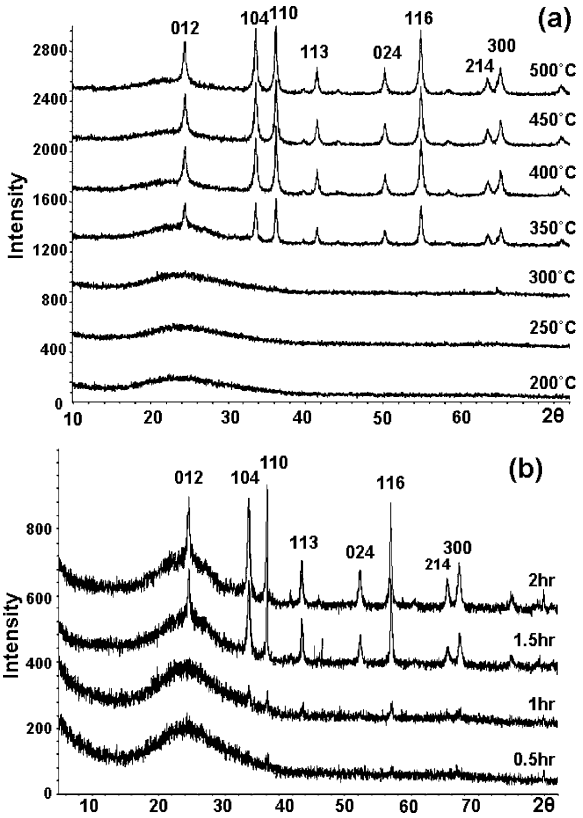

Figure 1. (a) XRD patterns of chromium nitrate loaded SBA-15 functioned with temperature. The heating time for each step was 5 h. The diffraction peaks are indexed to the rhombohedral Cr_2O_3, space group $R\bar{3}c$ with the unit cell parameters of $a = 0.4951$ and $c = 1.3598$ nm. (b) XRD patterns of specimens after heating chromium nitrate in SBA-15 at 350 °C with varying time.

3. Results and Discussion

3.1. Porous Single Crystals of Cr_2O_3. The specimen of $Cr(NO_3)_3{\cdot}9H_2O$-loaded SBA-15 has a green color, being characteristic of Cr^{3+} cations. It started to decompose at ~100 °C in air, and the color changed to brown, indicating that Cr^{3+} was oxidized into Cr^{4+}, while NO_3^- anions were reduced to NO_2 or NO. The brown color of the samples, characteristic for Cr^{4+}, became deeper when the heating temperature was increased up to 300 °C. The corresponding XRD patterns showed no crystalline phases (Figure 1a). It is therefore believed that the intermediate product of the decomposition of chromium(III) nitrate nonahydrate is a mixture of Cr(IV)-containing oxide and nitrate after a portion of the NO_3^- anions is reduced. The intermediate Cr(IV) oxide step can also be observed when chromium(VI) oxide reduces to Cr_2O_3.[20]

When the heating temperature was increased to 350 °C, the color of the specimens changed to a greenish brown,

(18) Xie, S. H.; Zhou, W. Z.; Zhu, Y. Q. *J. Phys. Chem. B* **2004**, *108*, 11561.
(19) Zhou, W. Z.; Klinowski, J. *Chem. Phys. Lett.* **1998**, *292*, 207.
(20) King, R. B. *Encyclopedia of Inorganic Chemistry* **1994**, *2*, 666.

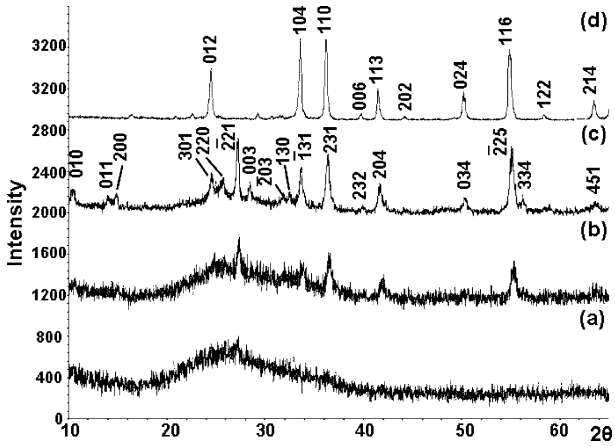

Figure 2. XRD patterns of the decomposition of $Cr(NO_3)_3 \cdot 9H_2O$ and crystallization of chromium oxide without using template. (a−c) XRD patterns of the specimens after heating $Cr(NO_3)_3 \cdot 9H_2O$ for 0.5−1.5 h, in 0.5 h increments, at 350 °C, respectively. Pattern (c) is indexed to Cr_2O_5 with a monoclinic unit cell with parameters $a = 1.201$, $b = 0.852$, $c = 0.939$ nm and $\beta = 92.0°$. (d) XRD pattern, after heating chromium nitrate at 400 °C for 5 h, showing the rhombohedral phase of Cr_2O_3.

implying a reduction of Cr^{4+} to Cr^{3+} had commenced, and crystallization of Cr_2O_3 occurred as indicated by the corresponding XRD pattern (Figure 1a), which can be indexed to the rhombohedral phase of Cr_2O_3, space group $R\bar{3}c$ with the unit cell parameters of $a = 0.4951$ and $c = 1.3598$ nm. The XRD results shown in Figure 1a are almost identical to the previous ones when $H_2Cr_2O_7$ was used as a precursor.[13] Nevertheless, it is obvious that the preparation procedure in the present work is much simpler.

From the XRD results and the color, it can clearly be seen that the crystallization of Cr_2O_3 started at 350 °C but was not completed even after 5 h. Another experiment of heat treatment of the $Cr(NO_3)_3 \cdot 9H_2O$-loaded SBA-15 at 350 °C in 0.5 h steps from 0.5 to 2 h was carried out. Although all four samples were brown in color indicating a high presence of Cr(IV), crystalline Cr_2O_3 obviously grew inside the SBA-15 channels. Figure 1b shows that very weak diffraction peaks of Cr_2O_3 appeared after heating for only 0.5 h and the peak intensity increased significantly when the heating time increased to 2 h. It can be concluded that rhombohedral Cr_2O_3 was the only crystalline phase developed during the heat treatment.

On the other hand, thermal decomposition behavior of $Cr(NO_3)_3 \cdot 9H_2O$ without the presence of the silica template is different. After a thermal treatment at 350 °C, no crystalline Cr_2O_3 was observed. Instead, an intermediate phase, Cr_2O_5, was detected after heating for 1 h (Figure 2b), and the intensity of the XRD peaks grew continuously with heating time (Figure 2c). Crystallization of Cr_2O_3 requires a higher temperature (Figure 2d).

Labus et al. recently reported their detailed decomposition studies of chromium nitrate.[21] It was found that the nitrate decomposed into a mix of amorphous chromium oxides with an average composition of about Cr_5O_{12} at the first stage of 300 °C. Chromium cations were oxidized when NO_3^- anions were reduced to gaseous phases NO_2 and NO. When the temperature was increased to above 415 °C, decomposition of Cr_5O_{12} led to the final product, Cr_2O_3, via several intermediate phases, such as Cr_2O_5 and CrO_2. The authors proposed that the thermal behavior of the above materials was dependent on a competition between two processes: reconstruction of the crystalline phase (endothermic effect) and recombination of the evolved atomic oxygen (exothermic effect). It was also found that when the mass of material decreased, a transition from exothermic to endothermic effects occurred.[21] In the present work, the limited space in the mesopores only allows a very small amount of chemicals to be involved in the decomposition and recrystallization. Furthermore, we expect the mesopore confinement effect would enhance an endothermic process and suppress an exothermic process due to the difficulty of heat transportation. Consequently, in the mesopores, Cr_2O_3 can form at a relatively lower temperature, and it is more difficult to form intermediate chromium oxides with higher oxidation states, such as Cr_2O_5 and CrO_2. A similar phenomenon was also found in the crystal growth of Co_3O_4 in mesoporous silicas as presented later.

To further investigate the formation mechanism of Cr_2O_3, the samples underwent HRTEM analysis. Although some weak XRD peaks of Cr_2O_3 had been observed from the sample after undergoing a heat treatment for less than 1 h at 350 °C (Figure 1b), the microcrystals of Cr_2O_3 in the SBA-15 channels were hardly detected by HRTEM imaging and selected area electron diffraction (SAED). This was as a result of the concentration of the crystals in the channels of SBA-15 silica being too low and the crystal size being too small with a high dispersion. In fact, very small metal clusters inside the mesopores of silica can be directly imaged easily when the concentration of the clusters is high, even if they are disordered or partially ordered.[22,23] SAED patterns from the 2 h sample revealed a multicrystal property (Figure 3a). This implies that the crystal growth began with a multiseed mode; i.e., many microcrystals were developed simultaneously in different channels of each SBA-15 particle.

Even after the sample was heated at 400 °C for 5 h and the crystallization was completed, as indicated by the XRD results, a polycrystalline property was still detected by SAED (Figure 3c), and these microcrystals could be seen as dark dots in the TEM images (Figure 3d) with diameters of 100 nm or less. The SAED patterns in Figure 3 also indicate that the crystals of Cr_2O_3 are randomly oriented inside the mesopores of SBA-15. Bearing in mind that the melting point of Cr_2O_3 is 2330 °C, the temperature applied was too low to allow recrystallization of the Cr_2O_3 crystallites into a larger crystal. Moreover, the crystallites are separated and immobilized by the SBA-15 mesopore network. The same results were also obtained from samples that had undergone thermal treatment at 550 °C for 5 h. Consequently, the final product, the so-called porous single crystals after the removal of the silica template, must have a much smaller size than

(21) Labus, S.; Malecki, A.; Gajerski, R. *J. Therm. Anal. Calorim.* **2003**, *74*, 13.

(22) Zhou, W. Z.; Thomas, J. M.; Shephard, D. S.; Johnson, B. F. G.; Ozkaya, D.; Maschmeyer, T.; Bell, R. G.; Ge, Q. *Science* **1998**, *280*, 705.

(23) Shephard, D. S.; Maschmeyer, T.; Johnson, B. F. G.; Thomas, J. M.; Sankar, G.; Ozkaya, D.; Zhou, W. Z.; Oldroyd, R. D.; Bell, R. G. *Angew. Chem., Int. Ed. Engl.* **1997**, *36*, 2242.

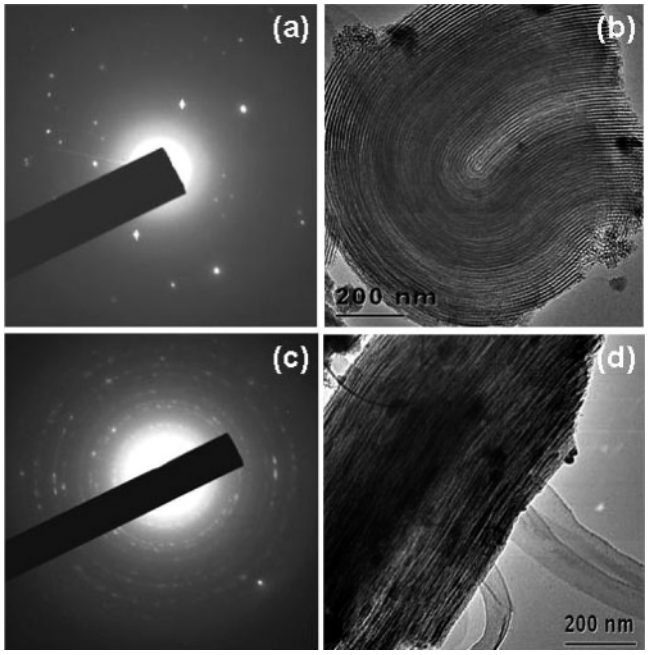

Figure 3. SAED pattern (a) of multicrystal Cr_2O_3 in a SBA-15 particle shown in the corresponding TEM image of (b) after a heat treatment for 2 h at 350 °C. (c and d) SAED pattern and the corresponding TEM image from the specimen after a heat treatment for 5 h at 400 °C, also showing the polycrystalline property.

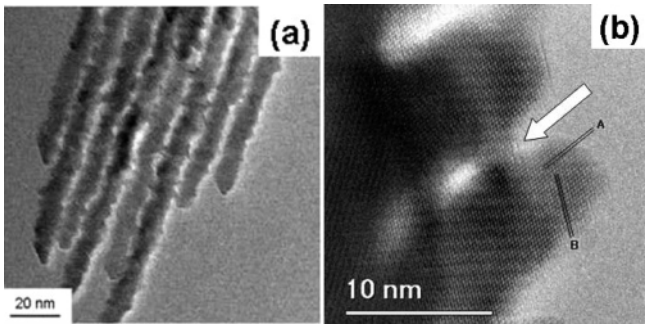

Figure 4. TEM (a) and HRTEM (b) images of some typical porous single crystals of Cr_2O_3 using SBA-15 as a template. Image (b) shows a nanobridge, indicated by the arrow, connecting two nanorods which have the same orientation of atomic planes. The *d* spacings of A and B are 0.250 and 0.2166 nm, corresponding to the $(\bar{1}23)$ and (110) planes, respectively, of the rhombohedral Cr_2O_3. The viewing direction is along the $[\bar{1}11]$ zone axis.

the size of the SBA-15 templating particles. Figure 4a shows a TEM image of a typical porous single crystal of Cr_2O_3. The crystal morphology, a group of straight nanorods connected by small bridges, is almost the perfect negative replica of the mesopore structure of SBA-15. The diameter of the particle is about 80 nm, much smaller than the average particle size of the SBA-15 template (Figure 3). Figure 4b shows the single-crystal property of the Cr_2O_3 particle, indicated by the uniform crystal orientation between the two nanorods and across the connecting bridge. This single-crystal property between all the nanorods can also be seen in our previously reported work.[13,17,24]

Unlike SBA-15, KIT-6 has a cubic symmetry, space group $Ia\bar{3}d$, and contains a 3D bicontinuous channel network.[4] In other words, there are two sets of identical mesopores

(24) Zhou, W. Z.; Zhu, K. K.; Yue, B.; He, H. Y.; Dickinson, C. *Stud. Surf. Sci. Catal.* **2004**, *154*, 924.

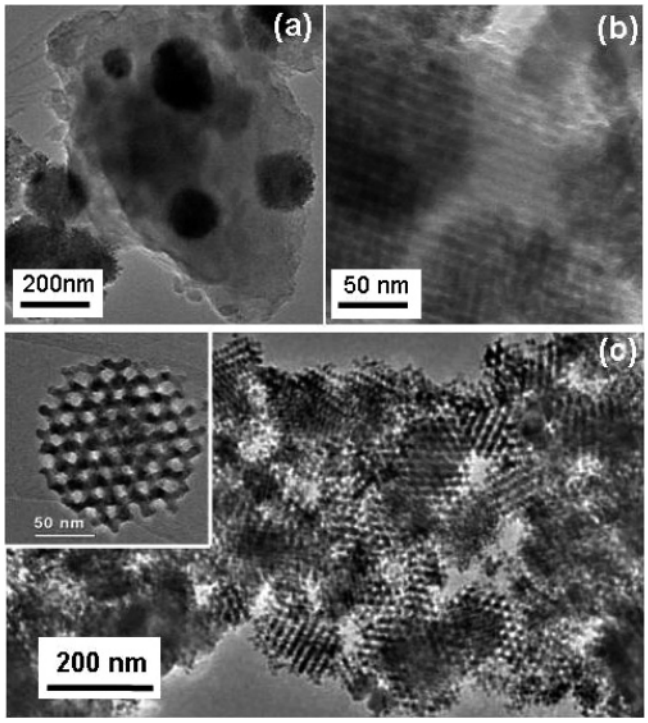

Figure 5. (a) Low magnification TEM image of a KIT-6 particle with several spherical Cr_2O_3 PSCs developed inside. (b) TEM image of the same specimen as part (a) with a higher magnification, showing mesopore fringes and separation of the Cr_2O_3 PSCs. (c) TEM image of Cr_2O_3 PSCs after the template has been removed. The inset shows a typical particle viewed down the [111] zone axis of the mesopore system.

coexisting in KIT-6 without any cross point. Chromium oxide crystals grown in KIT-6 for 5 h at 550 °C were also polycrystalline, similar to the results obtained from SBA-15 templated Cr_2O_3, in each KIT-6 particle, which was detected by SAED patterns. As shown in Figure 5a, one particle of KIT-6 contains several separated spherical PSC particles, with different particle sizes, which leads to the multicrystal diffraction pattern. After removing the silica template, the Cr_2O_3 PSCs have a spherical morphology, and their typical particle size is about 100−200 nm.[15] In Figure 5c, the range of the PSC particle sizes can clearly be seen. From each PSC particle, the SAED patterns and HRTEM images indicate a single-crystal feature.

TEM images shown in the inset of Figure 5c and Figure 6a indicate that the original mesopore system in KIT-6 has been replicated. However, the image-contrast patterns on both the [100] and [111] projections of the KIT-6 related unit cell show nanochannels along the view directions, implying that only one of the two sets of channels of KIT-6 was replicated. This structural feature has been confirmed in a comparison with the TEM images of the PSC Co_3O_4 and further supported by the pore volumes of two oxide PSCs obtained from nitrogen adsorption/desorption. HRTEM images, on the other hand, show that each particle is a single crystal. As a result, although several Cr_2O_3 nanorods overlapped but without connection to each other along the view direction, very good atomic images, as a single crystal, can still be observed as shown in Figure 6b, e.g., the areas indicated by the arrows.

Since we commonly observed from the PSCs of Cr_2O_3 prepared by a two-step method an excellent coherence in

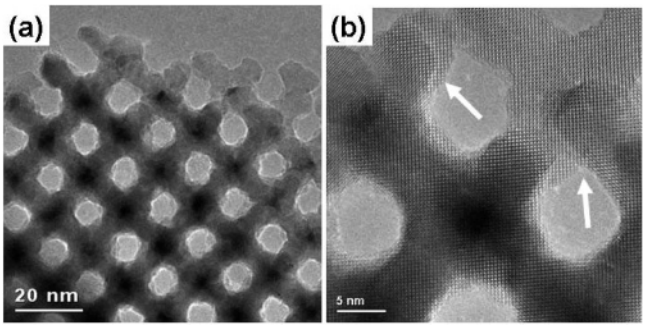

Figure 6. (a) TEM image of a porous single crystal of Cr_2O_3, showing the mesopore structure along the [100] zone axis of the KIT-related unit cell and (b) corresponding HRTEM image on the [$2\bar{2}1$] zone axis of the Cr_2O_3 unit cell. The two arrows indicate the PSC has the same crystal orientation at different parts of the mesoporous structure with various degrees of overlapping.

orientations between the Cr_2O_3 crystals and the KIT-6 mesopore structure, we suspected that the crystal orientation might be governed by the mesopore network, which could be regarded as a nanoreactor.[15] However, this phenomenon was not observed in other PSC specimens in the present work. On the other hand, the effect of mesopore networks of silica templates on the particle morphology of PSCs is obvious, e.g., a cylindrical shape of Cr_2O_3 PSC was developed in hexagonal SBA-15 and a spherical morphology dominates in the specimen when cubic KIT-6 is used as a template. As we can expect, TEM images indicated that the chromium oxide sample prepared without the presence of silica template has irregular shapes. The range of size was also very wide, from 150 nm to several micrometers in diameter. This offers further corroboration that the size and morphology of the PSC materials are controlled by the mesoporous template.

3.2. Porous Single Crystals of Co_3O_4. The thermal behavior of $Co(NO_3)_2 \cdot 6H_2O$ inside the silica mesopores is different from that of $Cr(NO_3)_3 \cdot 9H_2O$. The forming temperature for the cobalt oxide is relatively low, with cobalt oxide first appearing at 150 °C after 5 h. Figure 7a shows that when the temperature increased to 125 °C, some intermediate crystalline phases appeared which transformed to the Co_3O_4 crystals at 150 °C. The XRD patterns obtained from the specimens heated at and above 150 °C can be indexed using the face centered cubic unit cell of Co_3O_4, space group $Fd\bar{3}m$ with the lattice parameter $a = 0.8085$ nm (JCPDS 781970). No impurity phases were detected.

To investigate the intermediate phases, a $Co(NO_3)_2 \cdot 6H_2O$-loaded SBA-15 specimen was heated at temperature of 150 °C for different periods, i.e., 0.5−2 h with intervals of 0.5 h. After the thermal treatment for 0.5 h, the XRD pattern of the specimen looked very complicated (Figure 7b). It was found that the specimen contains two phases, $CoNO_3(OH) \cdot H_2O$ and $Co(NO_3)_2 \cdot 2H_2O$. The former has a monoclinic unit cell with $a = 1.7757$, $b = 0.3142$, $c = 1.4188$ nm and $\beta = 113.55°$, space group $P2_1/c$ (JCPDS 480091),[25] and the latter is also monoclinic with the unit cell parameters $a = 1.429$, $b = 0.6139$, $c = 1.2661$ nm and $\beta = 112.79°$, space group $I2/a$ (JCPDS 251219). The XRD pattern from the specimen

(25) Petrov, K.; Zotov, N.; Garcia-Martinez, O.; Rojas, R. *J. Solid State. Chem.* **1992**, *101*, 145.

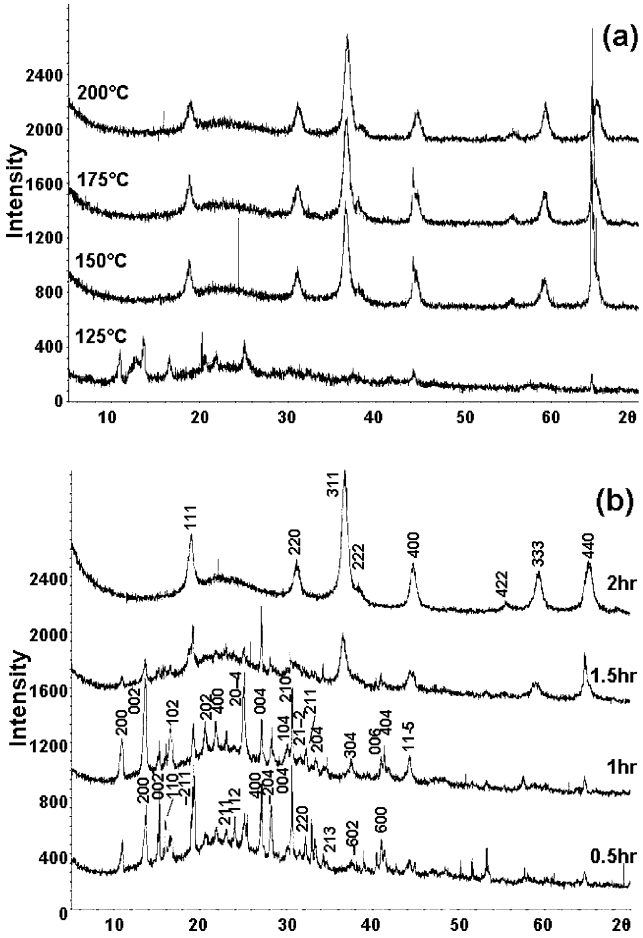

Figure 7. (a) XRD patterns of specimens with crystal growth of Co_3O_4 in KIT-6 functioned with temperatures at constant time of 5 h. (b) XRD patterns of specimens heated at constant temperature of 150 °C with varying time. The pattern with 1 h treatment is indexed to the monoclinic $CoNO_3(OH) \cdot H_2O$, and the pattern with 0.5 h treatment is indexed to the monoclinic $Co(NO_3)_2 \cdot 2H_2O$. The top pattern is indexed to the fcc Co_3O_4.

after the thermal treatment of 1 h also shows these two phases. However, the ratio of $CoNO_3(OH) \cdot H_2O/Co(NO_3)_2 \cdot 2H_2O$ increased notably. After the treatment of 1.5 h, the Co_3O_4 phase became the dominant phase, and after 2 h treatment, a pure phase of Co_3O_4 was obtained. Consequently, during the thermal treatment, crystallization of $Co(NO_3)_2 \cdot 2H_2O$ occurred first by the loss of four water molecules per $Co(NO_3)_2 \cdot 6H_2O$, followed by a phase transition to $CoNO_3(OH) \cdot H_2O$ by losing one NO_3^- anion and a proton. The crystallization of Co_3O_4 occurred at the final stage after the second NO_3^- anion and all water molecules were lost. The 2+ oxidation state of Co remained unchanged except in the final stage where it was partially oxidized into 3+.

The comparison of the decomposition of cobalt nitrate hexahydrate, with and without the presence of the mesoporous silica template, at the same temperature (150 °C) shows remarkably different results. The nontemplated specimen formed and stayed in the tetrahydrate state of the cobalt nitrate, $Co(NO_3)_2 \cdot 4H_2O$, even after a 5 h thermal treatment instead of forming cobalt oxide through the intermediate phases of cobalt nitrate dihydrate and cobalt hydroxide nitrate monohydrate (Figure 8a). Increasing the temperature to 200 °C, we still obtained $Co(NO_3)_2 \cdot 4H_2O$ as the only phase. At 225 °C, the cobalt nitrate started to break down to cobalt

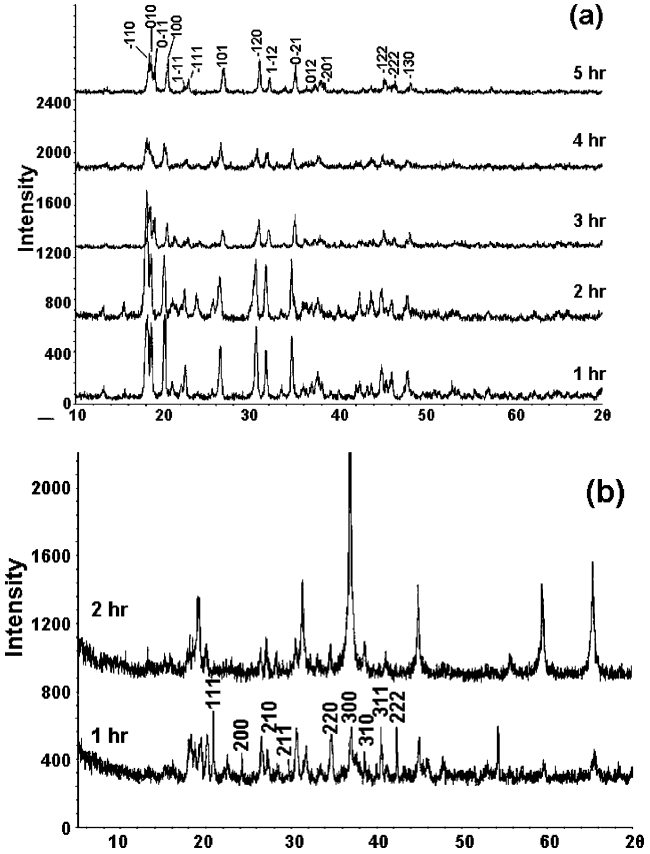

Figure 8. XRD patterns of the specimens after decomposing $Co(NO_3)_2 \cdot 6H_2O$ without the presence of silica template (a) at 150 °C for 1−5 h, and (b) 225 °C for 1 and 2 h. All patterns in part (a) can be indexed to triclinic $Co(NO_3)_2 \cdot 4H_2O$ with space group $P\bar{1}$ and unit cell parameters $a = 0.5516$, $b = 0.5996$, $c = 0.7228$ nm, $\alpha = 102.38°$, $\beta = 97.74°$, and $\gamma = 120.16°$. The pattern of 1 h treatment in part (b) shows a mixed phase of $Co(NO_3)_2 \cdot 4H_2O$ and $Co(NO_3)_2$; the peaks are indexed onto the latter, which has a primitive cubic unit cell with the parameter $a = 0.737$ nm. The other peaks belong to $Co(NO_3)_2 \cdot 4H_2O$. The pattern of 2 h treatment in part (b) shows the dominant phase of Co_3O_4 with some minor peaks from the intermediates.

oxide via two intermediate phases, $Co(NO_3)_2 \cdot 4H_2O$ and $Co(NO_3)_2$ (Figure 8b). Similar to the crystal growth of Cr_2O_3 as discussed above, the crystallization temperature of Co_3O_4 in the mesopores is significantly reduced. In addition, different intermediate phases were formed during the decomposition of the cobalt nitrate hexahydrate. It is noticed that the formation of $CoNO_3(OH) \cdot H_2O$ is not commonly observed. As discussed by Petrov et al. in 1992, the yield of $CoNO_3(OH) \cdot H_2O$, which normally only occurs on the outer crust of the decomposing nitrate, is extremely low as it is only a partial decomposition step.[25] It is as a result of this low yield that the crystal characterization had not been successful before their investigation. As well as the confinement and other effects described earlier in the paper, the increase in surface area of the cobalt nitrate, given by the mesopores, allows a higher yield which contributes to the appearance of such strong XRD peaks from not only $CoNO_3(OH) \cdot H_2O$ but also $Co(NO_3)_2 \cdot 2H_2O$.

SAED of the cobalt oxide PSCs within the template also revealed a polycrystalline property which suggested that many crystals developed with different orientations in the same particle of the KIT-6 template, which corroborates the above results from chromium oxide (Figure 3).

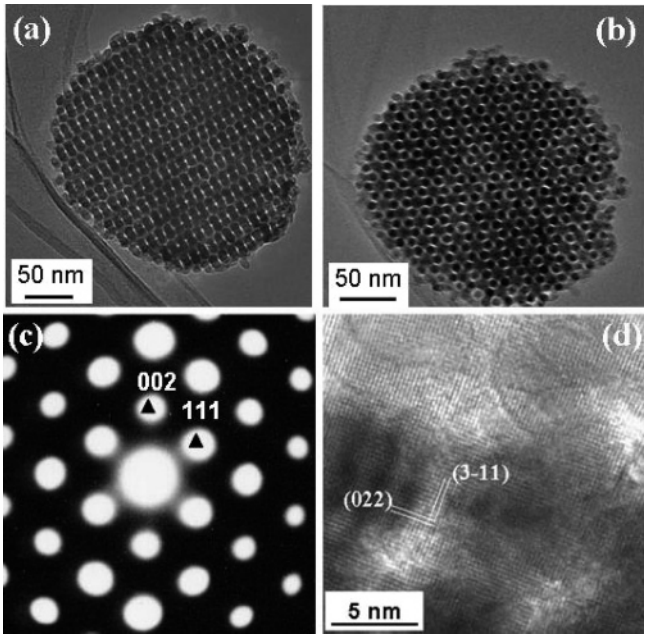

Figure 9. (a, b) Low magnification TEM images of Co_3O_4 PSCs templated by KIT-6 viewed down the [110] and [111] directions of the mesostructure, respectively. (c) A typical SAED pattern of Co_3O_4 PSCs viewed down the [$1\bar{1}0$] crystal orientation. (d) HRTEM image, viewed down the [$23\bar{3}$] direction, showing the single crystallinity of the PSCs.

Most particle sizes of the PSC Co_3O_4 ranged from 200 to 400 nm in diameter, whereas the KIT-6 particle size was several micrometers in size. The cobalt oxide forms a negative replica keeping the same space group as the template. The PSCs were spherical in shape indicating the crystal growth in a 3D mesopore system (Figure 9a,b). The SAED patterns and HRTEM images (Figure 9c,d) confirmed that each particle is a porous single crystal; i.e., all the parts (nanorods) in the particles have the same crystal orientation. Importantly, unlike the TEM images from PSC Cr_2O_3, no nanochannels can be directly projected along any principal zone axis of the KIT-6 related mesostructure, indicating that the whole bicontinuous channel network in KIT-6 has been replicated.

Because KIT-6 is several micrometers in size and there is no distinguishable environment from one area to the next, it stands to reason that the seed formation, occurring at many locations in the particle, is entirely random. However, once the PSC particle starts to form, and the amorphous material starts to migrate, it is more difficult for a new seed to form in its surrounding area. This is not always the case, as when two seeds form in close proximity to each other at approximately the same time, this can lead to the integration of the two mesoporous crystals when they meet. Figure 10a shows two spherical particles of PSC Co_3O_4 with their corresponding SAED patterns inserted. It can clearly be seen that both particles give single-crystal diffraction patterns with different zone axes, [$\bar{2}33$] for the left side particle and [$\bar{1}12$] for the right side particle. The area of integration can be estimated by comparing the double particle to the spherical shape of individual particles; this is indicated by the black arrow in Figure 10a. Figure 10b is an HRTEM image of the integration boundary of another two particles and reveals that both of the PSCs have their (113) planes perfectly aligned to each other. This may be the reason the integration

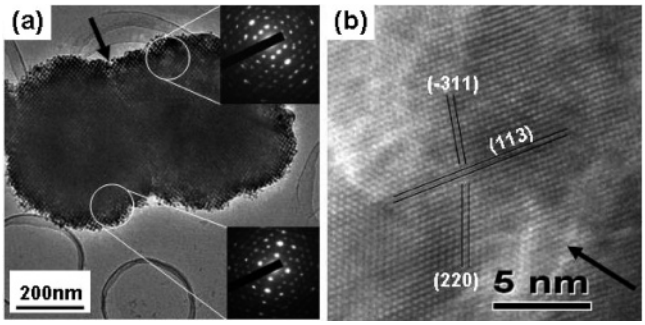

Figure 10. (a) TEM image of two Co_3O_4 PSCs with the same mesoporous framework but different crystal orientations as indicated by the SAED patterns (top right inset is the SAED pattern from the right-hand side particle with the zone axis [$\bar{1}$12], bottom right inset is the SAED pattern from the particle on left side with the zone axis [$\bar{2}$33]). The black arrow indicates the line of integration between the two particles. (b) HRTEM image of the integration point between another two PSCs. The pair of long black lines shows the common (113) plane that runs across the line of integration, indicated by the black arrow. The two pairs of shorter black lines on either side of the line of integration indicates the different plane of both the lower and upper particles, ($\bar{3}$11) and (220), respectively.

between the two crystal structures can take place, and although the zone axes are different, [1$\bar{1}$0] and [15$\bar{2}$], the commonality of the *d*-spacing is almost seamless. On the other hand, the mesopore network continues from one particle to the other perfectly as shown in Figure 10a. This can be easily understood as these combined double particles formed in the same KIT-6 particle. Since crystal growth of Co_3O_4 in KIT-6 used the two sets of mesopores, the chance of integration of two or more PSCs is higher in comparison with the PSCs of Cr_2O_3, in which only half of the bicontinuous channel network is replicated.

3.3. Nitrogen Adsorption/Desorption of Porous Single Crystals. The nitrogen adsorption/desorption experiment of KIT-6 (Figure S1) shows a typical type IV isotherm with H1 hysteresis expected for large pore mesoporous silicas with cylindrical pore geometry. There is a high affinity for nitrogen uptake with an adsorbed value of 758 cm^3/g (STP) and a total pore volume of 1.17 cm^3/g. The specific surface area is 752 $\pm$ 7 m^2/g, equivalent to 463 m^2/cm^3 if the density of silica is 2.2 g/cm^3. Sharp capillary condensation over a narrow relative pressure region of $P/P_0 = 0.7$ indicates the degree of ordering, as seen by TEM images (not shown), which is seen reflectively in both PSCs, corresponding to a mesopore size of 96 Å (inset of Figure S1). These values of the pores are similar to those given in the previous report.[4] There is another peak within the pore size distribution curve which has a maxima at 18 Å corresponding to ordered complementary pores; this is supported by information on the complementary pores in a paper by Sakamoto et al.[26] The micropore volume and surface area from the *t*-plot (Figure S2) are 0.034 cm^3/g and 72 m^2/g, respectively.

The isotherms of the PSCs show a reduction in nitrogen uptake down to 109 and 295 cm^3/g (STP) for the Co_3O_4 and Cr_2O_3 PSCs, respectively (Figure 11). This is due to an increase in the density, and also there is no evidence for microporosity from the *t*-plots (not shown). The rapid uptake of nitrogen within the Cr_2O_3 PSCs at high relative pressures

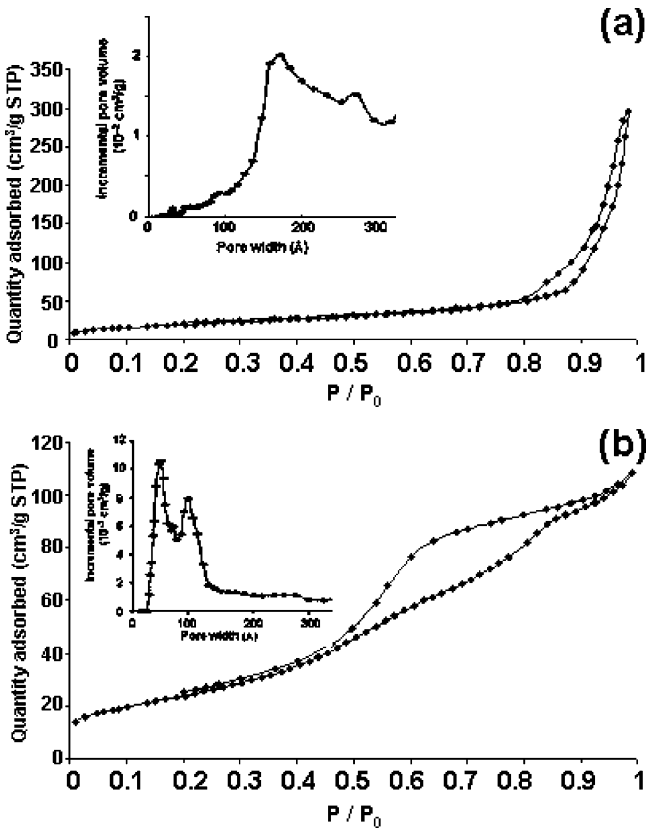

Figure 11. Nitrogen adsorption/desorption isotherms measured at 77 K from PSCs of (a) Cr_2O_3 and (b) Co_3O_4. Insets: pore size distributions via the DFT model assuming slit pore geometry.

($> P/P_0 = 0.88$) is presumably due to the relatively larger pores because only half of the channel network of KIT-6 was replicated. Condensation of the adsorbate between aggregated particles is another possible reason. The aggregation of particles after template removal for the Cr_2O_3 PSCs can be seen in the TEM image (Figure 5c) and is typical for the Cr_2O_3 product, and less common for the Co_3O_4 product which tends to have larger particles with better separation. The effect of the aggregation of particles can be seen in the isotherms of small AMS-8, which is comparable to the Cr_2O_3 isotherm and TEM images.[27]

Pore size distribution of the PSCs can be seen in the insets of Figure 11. There is some slight shape to the adsorption branch in the isotherm of the Co_3O_4 PSCs at around $P/P_0 = 0.5$ and again at 0.8, although not vertically steep (i.e., over a broad region), which gives rise to the peaks on the respective distribution curve at ~4 and ~9 nm that correlating to the broadness. The isotherm of the Cr_2O_3 PSCs is fairly linear up to the region of $P/P_0 = 0.88$, hence the broadness of the pore size distribution curve between 0 and 130 Å.

The specific surface areas and pore volumes (measured at relative pressures of $P/P_0 = 0.99$) of the Co_3O_4 PSCs are 92 m^2/g and 0.167 cm^3/g, and for Cr_2O_3 are 74 m^2/g and 0.456 cm^3/g. The surface area of Co_3O_4 PSCs can be written as 277 m^2/cm^3 when the density of Co_3O_4 is 6.07 g/cm^3, and the value for Cr_2O_3 PSCs is 114 m^2/cm^3 if the density

(26) Sakamoto, Y.; Kim, T. W.; Ryoo, R.; Terasaki, O. *Angew. Chem., Int. Ed.* **2004,** *43*, 5231.

(27) Garcia-Bennett, A. E.; Lund, K.; Terasaki, O. *Angew. Chem., Int. Ed.* **2006**, *45*, 2434.

of the oxide is 5.21 g/cm^3. The latter is less than 50% of the former, although the same template of KIT-6 was used for both PSCs. These results are in good agreement with the TEM observations that Cr_2O_3 PSCs only crystallized in one of the two channels in KIT-6 whereas Co_3O_4 PSCs developed in both channels. A possible reason for such a difference is the different crystallization conditions, which affect the stability of the complementary pores connecting the two channels. It is obvious that complementary pores are needed for good communication for an interconnected growth in both channels. If the complementary pores collapse, therefore causing the isolation of the two channels, then a one-channel growth, which can be seen in the Cr_2O_3 PSCs, will occur. Bearing in mind that the crystallization temperature for Co_3O_4 PSCs is 150 °C and that for Cr_2O_3 PSCs is 350 °C, the stability of the complementary pores inside the amorphous silica wall is reduced when the temperature increases. Moreover, during the crystallization, the crystals may create pressure on the silica wall and, therefore, also enhance the damage of the complementary pores. With the Co_3O_4 PSCs occurring at a low temperature, this pressure effect at the early growth stage does not affect the complementary pores to any great extent. However, with the increased temperature for the growth of the Cr_2O_3 PSCs, the less stable complementary pores are more likely to collapse with pressure, isolating the two channels and causing crystals in each to grow independently.

In summary, we investigated crystal growth of Cr_2O_3 and Co_3O_4 inside the mesopores in SBA-15 and KIT-6. Many seeds of nucleation were developed simultaneously at an early stage, and porous single crystals with 100−400 nm diameter were fabricated eventually after removing the silica templates. The morphologies of the PSC particles were affected by the mesopore systems. A significant confinement effect was observed to the decomposition of the metal nitrates and crystal growth of metal oxides inside the mesopores, which can be regarded as a nanoreactor, i.e., forming different intermediate phases and reduction of the crystallization temperature. Measurements of physical properties and catalytic activities of the new materials are under investigation.

Acknowledgment. W.Z. thanks EPSRC for the studentship for C.D. and Fudan University for the financial support for C.D.'s research visit to Fudan. C.D. thanks Dr. Philip J. Camp for his helpful discussion on the confinement effect and thanks Dr. Paul. A. Wright for his discussion on isotherms. D.Z. and H.H. thank NSF of China (20421303) for financial support.

Supporting Information Available: Nitrogen adsorption/desorption isotherms and *t*-plot for KIT-6. This material is available free of charge via the Internet at http://pubs.acs.org.

CM060014P